

**Karazin Kharkiv National University**  
**Department of Physics and Technology**



**Technische Universität Darmstadt**  
**Institut für Kernphysik**



**Design of a Shielding**  
**for the New Focal Plane Detector System**  
**of the Energy-Loss Spectrometer**  
**at the S-DALINAC**

**Diploma Thesis**

**Oleksiy Burda**

**Darmstadt 2002**

## **Abstract**

The investigation of the structure of the nucleus with inelastic electron scattering is one of the most important applications of the 130 MeV superconducting Darmstadt electron linear accelerator S-DALINAC at the Institute for Nuclear Physics of the Darmstadt University of Technology, Germany. In order to carry out high resolution electron scattering experiments especially with heavy nuclei, where the level densities are high, a new detector system is presently developed for the so-called energy-loss spectrometer. The old scintillator system is replaced by modern silicon-microstrip detectors.

During the experiments the detector system of the spectrometer has to be protected against neutrons and ionising radiation produced by neighbouring background sources by means of a passive radiation shielding. In the present work the design of such a shielding system is developed. Estimates of the total background produced by the typical background sources located near the spectrometer are presented. The requirements for the new shielding are defined. Also, the criteria of material choice for the shielding are considered. The estimates of the shielding thickness, necessary for reducing the background level down to a level of the proper detector operation are given. The working drawings of the designed shielding construction system are presented.

## Анотація

Дослідження структури ядра за допомогою непружного електронного розсіювання є одним з найважливіших використань надпровідного рециркулюючого лінійного прискорювача електронів S-DALINAC на 130 MeV в Інституті Ядерної Фізики (Дармштадський Технічний Університет, Німеччина).

Для того, щоб проводити експерименти по розсіянню електронів з високою роздільною здатністю, особливо з важкими ядрами, де щільність рівнів є високою, детекторна система спектрометра була змінена. Стара сцинтиляційна детекторна система була замінена на сучасні кремнієві мікрострипові детектори.

Під час експерименту, детекторну систему спектрометра потрібно захистити від нейтронів та іонізуючого випромінювання від найближчих радіаційних джерел пасивною радіаційною захисною спорудою. Розробка такої системи і є головною темою цієї дипломної роботи.

В рамках цієї роботи була зроблена оцінка сумарного фону біля детекторної системи спектрометра. Були пред'явлені вимоги до нової радіаційної захисної споруди. Також даються критерії вибору матеріалів для захисту детекторної системи від фотонів та нейтронів. Представлені оцінки товщини захисного матеріалу, які необхідні для зменшення фону до рівня, який забезпечує належну роботу електронної частини детекторної системи за допомогою коефіцієнтів десятичного ослаблення випромінювання. Також даються креслення розробленої захисної споруди.

# *Contents*

<b>1 . Introduction .....</b>	<b>5</b>
<b>2 . S-DALINAC and experimental facilities .....</b>	<b>6</b>
<b>3 . Production and attenuation of background radiation .....</b>	<b>8</b>
<b>3.1 Bremsstrahlung yield from a target.....</b>	<b>8</b>
<b>3.2 Attenuation of gamma radiation.....</b>	<b>12</b>
<b>3.3 Photoneutron reactions and neutron yield from a target .....</b>	<b>15</b>
<b>3.4 Slowing down and capture of neutrons.....</b>	<b>18</b>
<b>4 . The energy-loss spectrometer.....</b>	<b>20</b>
<b>4.1 High resolution electron scattering facility.....</b>	<b>20</b>
<b>4.2 Matrix formalism and ion-optical properties of the spectrometer .....</b>	<b>24</b>
<b>4.3 Energy-loss mode.....</b>	<b>25</b>
<b>4.4 New detector system.....</b>	<b>27</b>
<b>5 . Shielding design .....</b>	<b>28</b>
<b>5.1 Background sources and estimates of total background radiation at the     detector system .....</b>	<b>28</b>
<b>5.1.1 Photon and neutron yields from the 70° bending magnet .....</b>	<b>31</b>
<b>5.1.2 Photon and neutron yields from the target .....</b>	<b>32</b>
<b>5.1.3 Photon and neutron yields from the post-target system. ....</b>	<b>33</b>
<b>5.1.4 Total instrumental background.....</b>	<b>35</b>
<b>5.2 Requirements to the new shielding system .....</b>	<b>35</b>
<b>5.3 Choice of the optimal shielding materials.....</b>	<b>36</b>
<b>5.4 Estimates of the necessary shielding thickness.....</b>	<b>38</b>
<b>6 . Construction of the shielding .....</b>	<b>40</b>
<b>7 . Conclusion .....</b>	<b>43</b>
<b>8 . References .....</b>	<b>44</b>

## 1. Introduction

The investigation of the structure of the nucleus with inelastic electron scattering is one of the most important applications of the superconducting Darmstadt electron linear accelerator S-DALINAC at the Institute of Nuclear Physics of the Darmstadt University of Technology. Due to its modern concept the S-DALINAC is a high quality source of continuous electron beams with energies up to 130 MeV. For momentum analysis of the scattered on the target electrons in nuclear physics experiments the so-called QCLAM spectrometer is used. Due to its large solid angle and momentum acceptance this spectrometer is well suited for  $(e,e'x)$  coincidence and  $180^\circ$  scattering experiments [1-3].

Additionally, a spectrometer for high resolution  $(e,e')$  experiments which was already used with the old normal-conducting accelerator DALINAC [4-7] is available. This spectrometer is operated in a so-called “energy-loss” mode. The main advantage of this mode is that the resolution of the electron scattering experiment does not depend on the energy spread of the primary electron beam. In order to carry out high resolution electron scattering experiments especially with heavy nuclei, where the level densities are high, a new detector system is presently developed at the spectrometer [8]. The old scintillator system is replaced by a modern silicon microstrip detector.

During the experiments the detector system of the spectrometer has to be protected against neutrons and ionising radiation by the radiation shielding. The new detector system requires a new shielding design. Development, construction and installation are the aim of this diploma thesis.

## 2. S-DALINAC and experimental facilities

The S-DALINAC was constructed at the Institute for Nuclear Physics of the Darmstadt University of Technology [9]. It became the first superconducting continuous-wave linear accelerator of electrons in Europe. Since 1991 the S-DALINAC delivers electron beams with the maximum energy of 120 MeV and currents of up to  $60 \mu\text{A}$  for a wide range of experiments. The layout of the S-DALINAC is shown in Fig. 1.

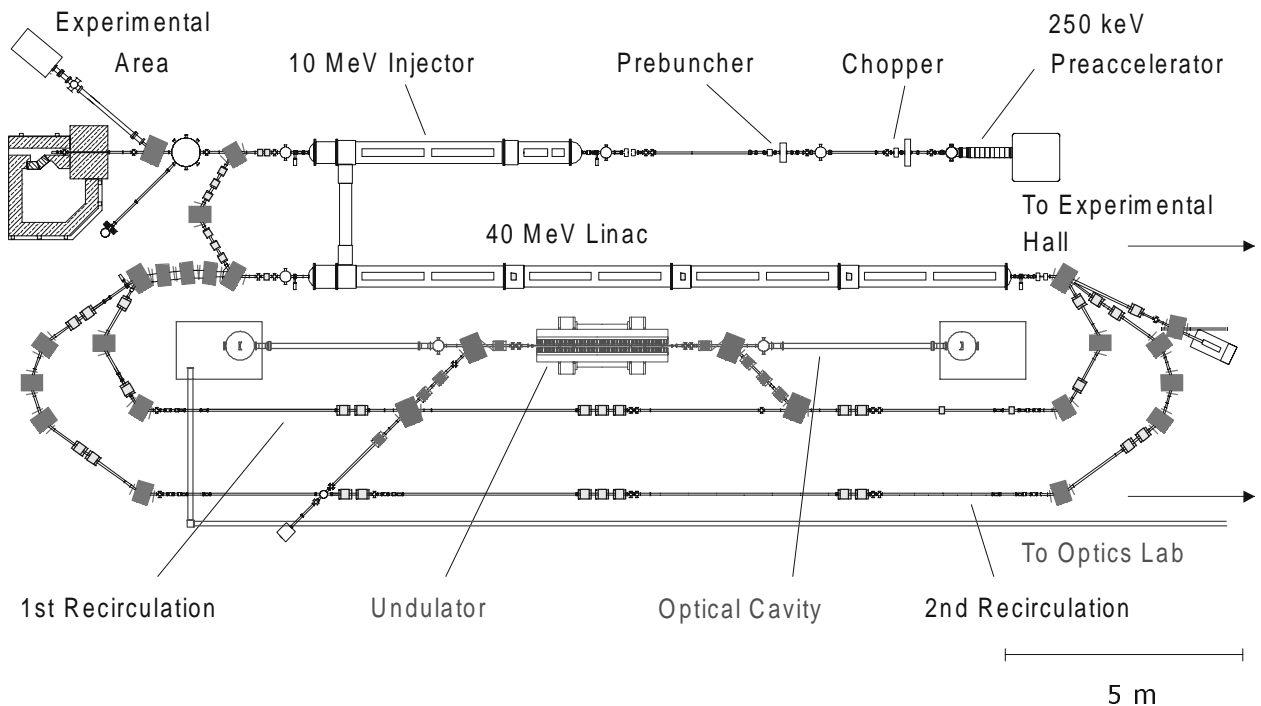
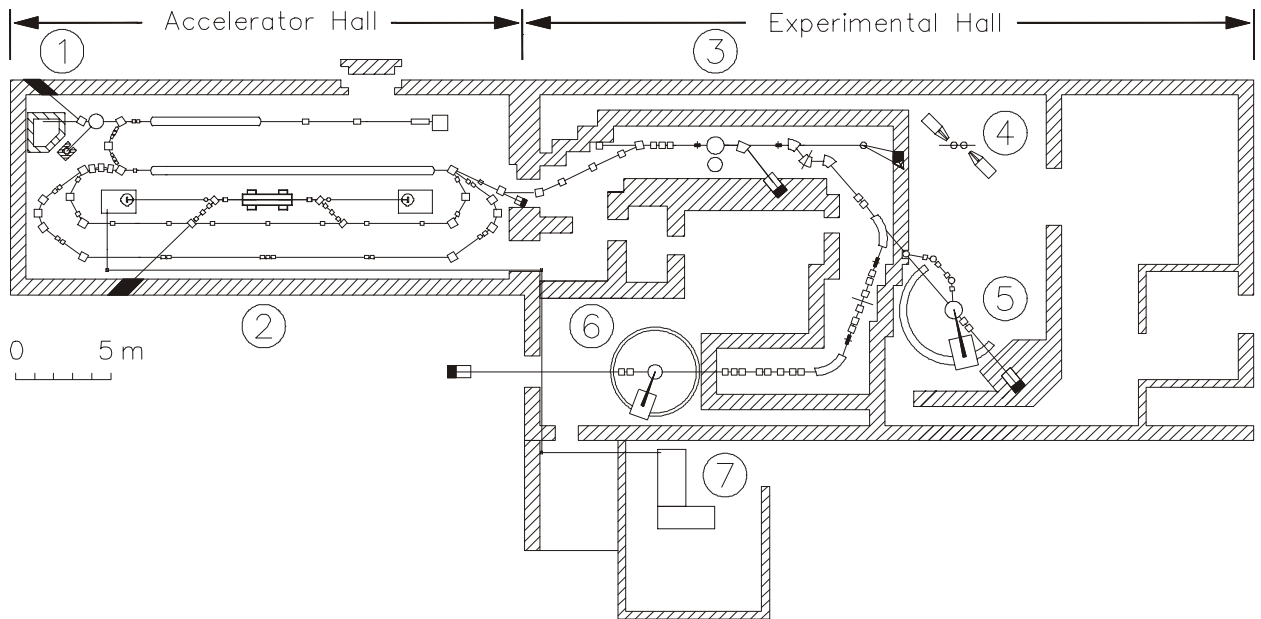


Fig. 1: Schematic layout of the S-DALINAC.

The electrons are emitted by a thermionic gun and then accelerated electrostatically to an energy of 250 keV. The required time structure of the electron beam for radio-frequency acceleration in a 3 GHz field is created by a chopper/prebuncher system operating at room temperature. The superconducting injector linac consists of one 2-cell, one 5-cell, and two standard 20-cell niobium cavities cooled to 2 K by liquid helium. The beam leaving the injector has an energy up to 10 MeV and can either be used for radiation physics experiments or for nuclear resonance fluorescence experiments. Alternatively, it can be bent by  $180^\circ$  and injected into the main accelerator section. This superconducting linac has

eight 20-cell cavities which provide an energy gain of up to 40 MeV. After passing through the main linac the electron beam may be extracted to the experimental hall or it can be recirculated and reinjected one or two times. Additionally, in the first recirculation beam-line an infrared Free Electron Laser (FEL) is located. After three passes the electron beam with a maximum energy of up to 130 MeV is delivered to several experimental facilities, schematically shown in Fig. 2.



**Fig. 2:** Experimental facilities at the S-DALINAC.

1 - channeling radiation and  $(\gamma, \gamma')$  experiments, 2 - Free Electron Laser, 3 - high energy radiation physics, 4 - Compton scattering off nucleons 5 -  $(e, e')$  at  $180^\circ$  and  $(e, e'x)$  experiments, 6 -  $(e, e')$ -experiments, 7 - optic experiments.

A wide range of electron scattering experiments is carried out using the QCLAM spectrometer (Pos. 5) and a high resolution energy-loss facility with a magic-angle spectrometer (Pos. 6). The QCLAM-spectrometer has a large angular and momentum acceptance and is used for  $(e, e'x)$  coincidence and  $(e, e')$  at  $180^\circ$  experiments. The magic-angle spectrometer operates in the so-called “energy-loss” mode that enables to perform high resolution  $(e, e')$  experiments independently of the energy spread of the electron beam.

### 3. Production and attenuation of background radiation

The main secondary effects produced by the passage of charged particles through matter are the excitation and ionization of atoms, and emission of photons and ejection of neutrons from nuclei. The first two phenomena can be considered as the result of a direct interaction between the primary particles and atomic electrons, and may be referred to as non-radiative collision processes, or, shortly, as collision processes. The emission of photons is caused by the deceleration of the primary particle in the Coulomb field of the nucleus. This process may be denoted as a radiative collision process, or, shortly, as a radiation process.

Therefore, the total energy loss of electrons is composed of two parts

$$\left(\frac{dE}{dx}\right)_{tot} = \left(\frac{dE}{dx}\right)_{rad} + \left(\frac{dE}{dx}\right)_{coll}. \quad (1)$$

Photons are radiated from any object struck by the primary electrons and form an external secondary beam. In a situation where photons are incident on matter there are three main processes: photoelectric effect, Compton effect, and pair production. The probability of electron-positron pair production rises with increasing photon energy and becomes important at energies above about 5 MeV in high-Z materials. Thus, the phenomenon of the electromagnetic shower or cascade occurs [10]. At high energies this phenomenon plays a dominant role in the description of the energy loss. Furthermore, background neutrons can be produced via photonuclear reactions.

In this section all these processes will be described more detailed.

#### 3.1 Bremsstrahlung yield from a target

When a swiftly moving charged particle of mass  $m$  and charge  $z$  passes close to a nucleus of charge  $Z$ , it experiences a Coulomb force proportional to  $z \cdot Z$  and consequently undergoes an acceleration proportional to  $z \cdot Z/m$ . According to

classical physics, an accelerated charge radiates electromagnetic energy at a rate proportional to  $z^2 \cdot Z^2/m^2$ . The proportionality to the square of the atomic number means that the loss of energy by radiation should be much more important in heavy elements than in light ones, while the inverse proportionality to the square of mass implies that light particles should radiate much more readily than heavy ones. Consequently, radiation as an energy loss mechanism is usually significant for electrons only.

The bremsstrahlung-energy spectrum extends from zero to the full initial energy of the electrons. Typical distributions for a number of electron energies in platinum ( $Z=78$ ) are shown in Fig. 3 [11].

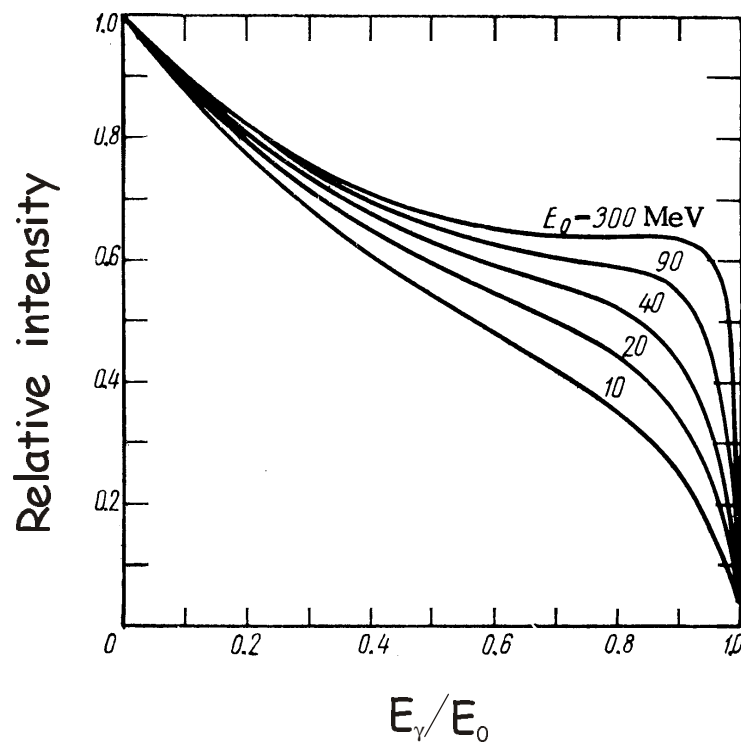


Fig. 3: Bremsstrahlung spectrum for various electron energies in platinum [11].

The average opening angle of the emission cone of bremsstrahlung photons at relativistic energies is given approximately by the well-known formula

$$\bar{\theta} \approx \frac{mc^2}{E_0} \quad (2)$$

where  $E_0$  is the initial energy of the electron.

As pointed out above, the rate of energy loss by radiation is roughly proportional to the square of the atomic number of the stopping material. It also increases rapidly with the energy, being negligible below 100 keV and rising to values greater than the rate of loss by collision at energies between 10 and 100 MeV, depending on the material. In the relativistic limit  $E_0 \gg 137mc^2 Z^{-1/3}$ , where the screening of the nuclear charge by the atomic electrons is complete, the rate of loss is given by [12]

$$-\left(\frac{dE}{dx}\right)_{rad} = 4Z(Z+1)r_0^2 n \alpha E_0 \ln(183Z^{-1/3}), \quad (3)$$

where  $n$  is the number of target atoms per  $\text{cm}^3$ ,  $\alpha$  is the fine structure constant, and  $r_0$  is the classical electron radius.

The bremsstrahlung energy loss is proportional to the initial energy of electrons as shown in Fig. 3. The energy at which the losses due to collision and bremsstrahlung for electrons are the same

$$\left(\frac{dE_c}{dx}\right)_{rad} = \left(\frac{dE_c}{dx}\right)_{coll} \quad (4)$$

is called critical energy  $E_c$ . Above this energy radiation loss will dominate over collision-ionization losses. An approximate formula for  $E_c$  is given by [13]

$$E_c = \frac{800}{Z+1.24} [\text{MeV}]. \quad (5)$$

The ratio of the radiation loss to the collision loss at the energy  $E_0$  is about

$$\frac{(dE/dx)_{rad}}{(dE/dx)_{coll}} \approx \frac{E_0 \cdot Z}{1600 \cdot mc^2}. \quad (6)$$

It can be seen from Eq. (6) that, whereas in graphite ( $Z = 6$ ) the radiation loss becomes comparable to the collision loss only at energies above 100 MeV, in lead ( $Z = 82$ ) these two are equal already at about 10 MeV.

Above the critical energy the electrons will lose their energy according to

$$E = E_0 \cdot \exp\left(-\frac{x}{L_{rad}}\right), \quad (7)$$

where  $x$  is the distance traveled and  $L_{rad}$  is the radiation length. For quick calculations, the following convenient expression for  $L_{rad}$  can be used [12]

$$L_{rad} = \frac{716.4 \cdot A}{Z(Z+1) \ln(287/\sqrt{Z})} \left[ \frac{g}{cm^2} \right], \quad (8)$$

where  $A$  is the mass number of the target.

Using the atomic model of Thomas and Fermi, Schiff [14] obtained the following expression for the bremsstrahlung cross section for full screening and relativistic energies of the incident electrons

$$d\sigma_{\gamma}(E_{\gamma}, \theta_0) = \frac{8Z(Z+1)r_0^2}{137} \cdot \frac{dE_{\gamma}}{E_{\gamma}} \cdot \frac{E_0 - E_{\gamma}}{E_0} \cdot \frac{xdx}{(1+x^2)^2} \cdot \left\{ \left[ \frac{E_0}{E_0 - E_{\gamma}} + \frac{E_0 - E_{\gamma}}{E_0} - \frac{4x^2}{(1+x^2)^2} \right] \times \right. \\ \left. \times \ln \left( \frac{2E_0(E_0 - E_{\gamma})}{m_0c^2 \cdot E_{\gamma}} \right) - \frac{1}{2} \left[ \frac{E_0}{E_0 - E_{\gamma}} + \frac{E_0 - E_{\gamma}}{E_0} + 2 - \frac{16x^2}{(1+x^2)^2} \right] \right\} \quad (9)$$

Here,  $x = \frac{E_0}{m_0c^2} \cdot \theta$  is the reduced photon emission angle.

The total photon yield in the thin-target approximation can be expressed as follows

$$Y_{\gamma} = \frac{N_a}{A} \cdot N_e \cdot t \cdot \int_0^{E_0 - mc^2} \int_0^{\theta_0} d\sigma_{\gamma}(E_{\gamma}, \theta_0), \quad (10)$$

where  $N_a$  is Avogadro's number,  $N_e$  is the number of electrons hitting the target,  $t$  is the target areal density.

The radiation yield for electrons stopped in various media is shown in Fig. 4 [15].

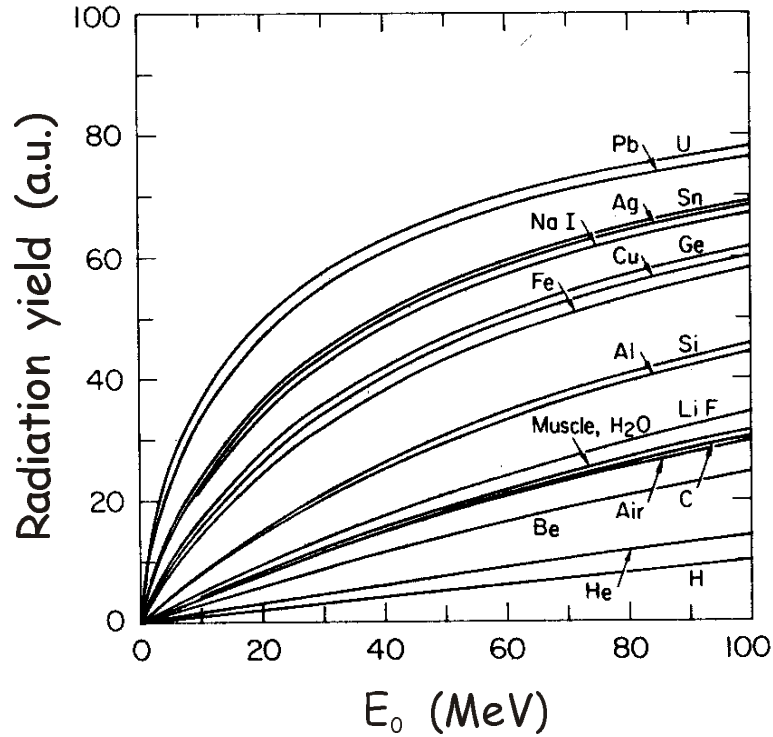


Fig. 4: The radiation yield for electrons stopped in various media [ 15].

### 3.2 Attenuation of gamma radiation

As was mentioned above, high energy photons traversing matter undergoes the following secondary processes:

*Photoelectric effect:* absorption by an atom accompanied by the emission of a high energy electron from the atom. Though the photoelectric effect becomes less and less important with increasing photon energy, even at MeV energies the dependence of the cross section per atom,  $\sigma_{ph}$ , scales with  $Z^5$ . Clearly, higher  $Z$  materials are most favoured for photoelectric absorption.

*Compton effect:* scattering of photons on free electrons. In this case the cross-section  $\sigma_c$  depends linearly on atomic number  $Z$ .

*Pair production,* i.e., transformation of photon energy into an electron and a positron. In this case the cross section per atom is proportional to  $Z^3$ .

The energy dependences of these processes for lead are shown in Fig. 5.

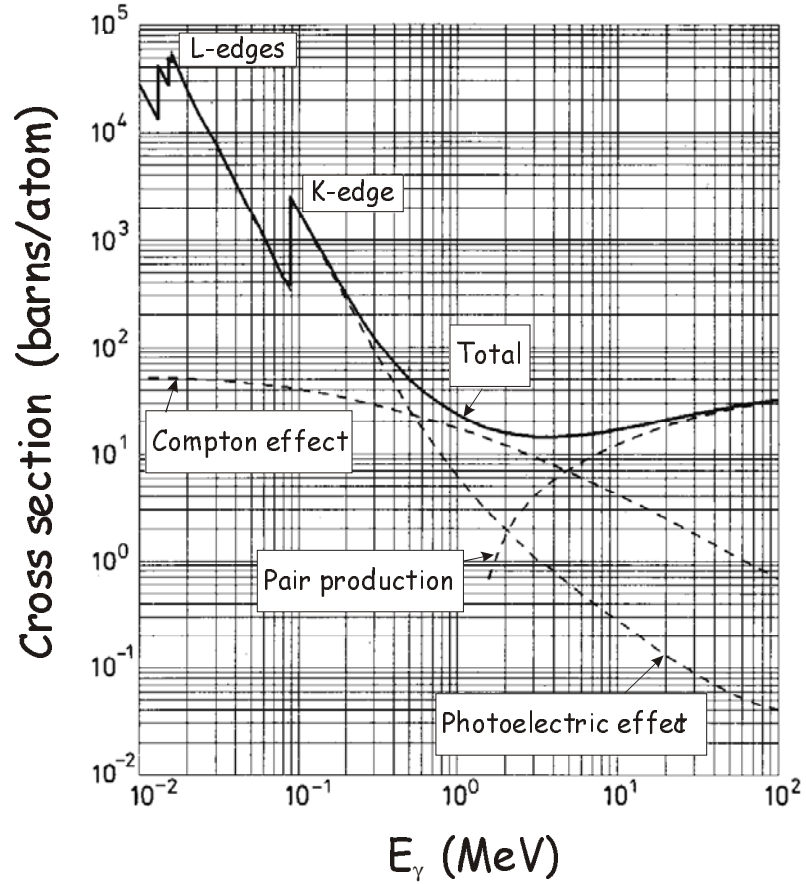


Fig. 5: The photon absorption cross section for lead [12].

The intensity of a narrow photon beam passing through a material with a thickness  $t$ , reduces exponentially

$$I = I_0 \cdot e^{-\mu_{tot}t}, \quad (11)$$

where  $I_0$  is the initial intensity of the monoenergetic photon flux interacting with matter, and  $\mu_{tot}$  represents the total linear attenuation coefficient, which is given by

$$\mu_{tot} = \rho \frac{N_A}{A} \cdot (\sigma_{ph} + \sigma_c + \sigma_{pair}). \quad (12)$$

Here  $\sigma_{ph}$ ,  $\sigma_c$ , and  $\sigma_{pair}$  are the cross sections for the photoelectric effect, Compton scattering, and pair production, respectively, and  $\rho$  is the density of the material.

For compounds and mixtures the total attenuation coefficient may be calculated using Bragg's rule

$$\frac{\mu}{\rho} = \omega_1 \frac{\mu_1}{\rho_1} + \omega_2 \frac{\mu_2}{\rho_2} + \dots, \quad (13)$$

where  $\omega_i$  is the weight fraction of each element in the compound. The linear absorption coefficient  $\mu$  is proportional to the density of the absorbing material. It is often more convenient to deal with the mass attenuation coefficient,  $\mu/\rho$  which is approximately independent of the material properties. It is a function of the photon energy but not of the radiation intensity or material thickness.

In practice and in the discussions presented in this diploma thesis the concept of tenth-value layers (TVL) is used for estimates of the shielding thickness against bremsstrahlung and neutrons. A TVL is defined as the thickness of absorber that will reduce the intensity of a narrow beam of the radiation by a factor of ten. When the attenuation is exponential, the tenth-value layer is given by

$$TVL = \frac{\ln 10}{\left( \frac{\mu_{tot}}{\rho} \right)} \left[ \frac{g}{cm^2} \right]. \quad (14)$$

The simple exponential attenuation described by Eq. (11) is observed only for a monoenergetic photon beam. When photons of more than one energy are present, the net attenuation coefficient is determined by weighting with the spectrum of photon energies. However, for practical purposes the TVL originally developed for dose considerations remains a useful approximation for particle intensities as well.

The photon and neutron tenth-value layers of various shielding materials are given in Tab. 1. One can see that lead is the most effective attenuator of photons and polyethylene is that of neutrons.

**Tab. 1:** The photon and neutron tenth-value layers of different shielding materials [16-18].

<b>Material</b>	<b>Density [g/cm<sup>3</sup>]</b>	<b>TVL<sub>γ</sub> [cm]</b>	<b>TVL<sub>n</sub> [cm]</b>
Pb	11.35	5	33
Fe	7.87	10	30
Concrete	2.35	48	40
Polyethylene	0.93	173	16

### 3.3 Photoneutron reactions and neutron yield from a target

Above a threshold energy which varies from about 10 to 19 MeV for light nuclei and from 6 to 8 MeV for heavy nuclei, neutron production will take place in any material hit by an electron or bremsstrahlung beam. The produced neutrons may present a radiation hazard by themselves and are also a source of induced activity.

Between the threshold and approximately 30 MeV, neutron production results primary from a process known as excitation of the giant dipole resonance (GDR). The physical mechanism can be described as one in which the electric field of a photon transfers its energy to the nucleus by inducing an oscillation in which the protons as a group move oppositely to the neutrons as a group. The cross section of GDR has a maximum at photon energies of approximately 20-23 MeV for light nuclei ( $A \leq 40$ ), and 13-18 MeV for medium and heavy nuclei. For  $A \geq 40$ , the energy of the peak is approximately given by

$$E_{\gamma_0} = 80 \cdot A^{-1/3} \text{ MeV}. \quad (15)$$

This phenomenon occurs in all nuclei (except  $^1\text{H}$ ). The width of this peak varies between 3 MeV (heavy nuclei) and 10 MeV (light nuclei).

In the semiclassical theory of the interaction of photons with nuclei, the shape of a resonance in the absorption cross section as a function of the photon energy  $E_\gamma$  has the form of a Lorenz distribution [19]

$$\sigma_n(E_\gamma) = \frac{\sigma_{\max}}{1 + \left( \frac{E_\gamma^2 - E_{\gamma 0}^2}{E_\gamma \cdot \Gamma} \right)^2}, \quad (16)$$

where  $\sigma_{\max}$  is the maximum cross section (in barns) of the giant resonance,  $E_{\gamma 0}$  and  $\Gamma$  are the photon energy for  $\sigma_{\max}$  and full width at half maximum of the cross section in MeV, respectively. The absorption cross section of  $^{208}\text{Pb}$  as a function of the photon energy is shown in Fig. 6 [20, 21].

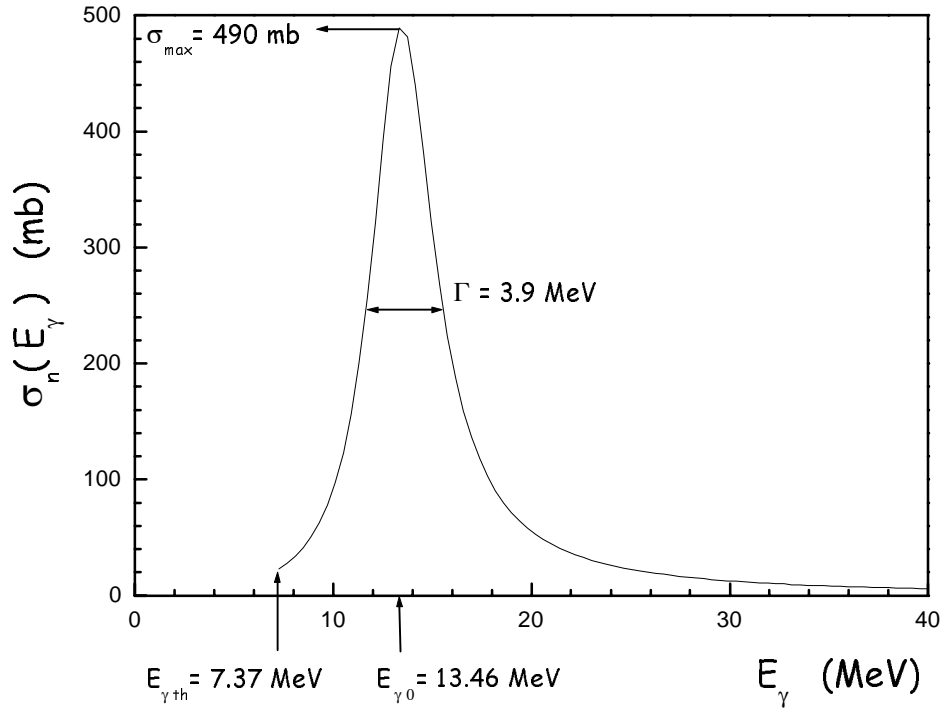


Fig. 6: Photoneutron cross section of  $^{208}\text{Pb}$  as a function of photon energy [20, 21].

The neutron yield from bremsstrahlung in the thin-target approximation can be obtained from the following expression

$$Y_n = t \cdot \frac{N_a}{A} \cdot \int_{E_{\gamma th}}^{E_{\gamma max}} \sigma_n(E_\gamma) \cdot \frac{dY_\gamma(E_\gamma)}{dE_\gamma} dE_\gamma, \quad (17)$$

where  $E_{\gamma th}$ ,  $E_{\gamma max}$  are the threshold energy and maximum photon energy for giant resonance.

The typical situation at electron accelerators corresponds to thick targets. In this case one has to perform numerical simulations. Neutron yields from semi-

infinite targets per unit electron beam power are plotted in Fig. 7 as a function of the electron beam energy [22].

The produced neutrons exhibit a roughly isotropic angular distribution with a Maxwellian energy distribution

$$\frac{dY_n}{dE_n} = \frac{E_n}{T^2} e^{-E_n/T}, \quad (18)$$

where  $T$  is a parameter characteristic of the target nucleus ( e.g.  $T = 0.98$  MeV for lead).

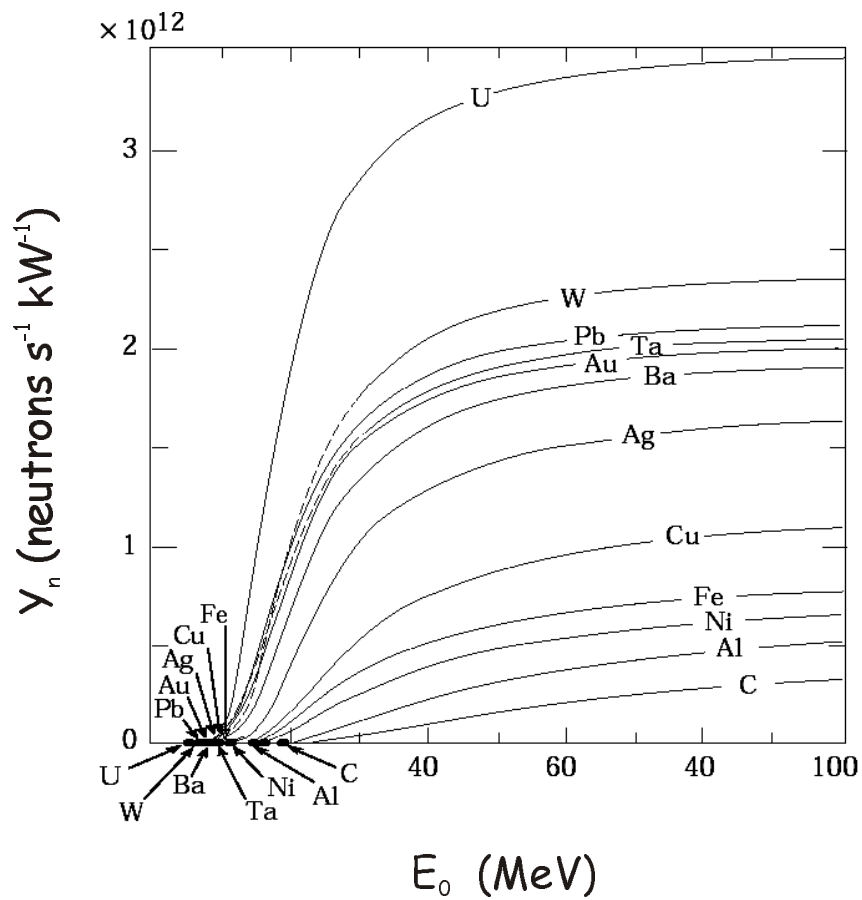


Fig. 7: Neutron yields from semi-infinite targets per kW of electron power as a function of electron beam energy, disregarding target self-shielding [22].

### 3.4 Slowing down and capture of neutrons

Passing through matter, the neutrons undergo a variety of nuclear processes depending on their energy. Among them are:

1. Elastic scattering from nuclei, i.e. reactions  $A(n,n)A$ . This is the most important mechanism of energy loss for neutrons in the MeV region. The maximum energy that can be transferred to a nucleus of mass number  $A$  by a neutron of energy  $E_n$  is given by

$$\left(\frac{\Delta E}{E_n}\right)_{\max} = \frac{4A}{(A+1)^2}, \quad (19)$$

where  $\Delta E$  is the energy lost by a neutron, and  $E_n$  is the initial neutron energy.

The average loss of energy in an elastic collision is the largest when the neutron is scattered off a hydrogen nucleus [12]. It is found that the average logarithmic energy loss suffered by a neutron of initial energy  $E_n$  in a collision with nucleus of mass number  $A$  is

$$\xi = \overline{\ln E_n - \ln E} = 1 + \frac{(A-1)^2}{2A} \ln\left(\frac{A-1}{A+1}\right). \quad (20)$$

This value does not depend upon the initial neutron energy and is a constant for a given material. Therefore, this quantity is convenient for estimating the moderating ability of a material.

The average number of collisions needed to reduce the neutron energy from an initial value  $E_0$  to a lower energy  $E$  is given by

$$n = \frac{\ln(E_0/E)}{\xi}. \quad (21)$$

Thus, e.g. the average number of collisions necessary to reduce the energy of the neutron from 2 MeV down to 0.025 eV (thermal energy) in hydrogen is only 18, in graphite is over 100, and in lead is already about 2000.

2. Inelastic scattering, i.e.  $A(n,n')A^*$ ,  $A(n,2n')B$ , etc. In this reaction the nucleus is left in an excited state which decays by gamma rays or some particle emission (if

energetically allowed). In order for the inelastic scattering to occur, the neutron must have sufficient energy to excite the nucleus, usually of the order of 1 MeV or higher. Below this energy threshold, only elastic scattering may occur.

3. Radiative neutron capture, i.e. a reaction  $n + (Z, A) \rightarrow \gamma + (Z, A+1)$ . In general, the cross section for neutron capture goes approximately as  $\approx 1/v$ , where  $v$  is the velocity of the neutron. Absorption is most likely, therefore, at low energies. Extremely high thermal neutron absorption cross sections are provided e.g. by boron, cadmium and gadolinium.

In the design of a passive radiation shielding it is necessary to take into account the fact that neutron elastic scattering and neutron capture are generally accompanied by the production of secondary gamma rays. Therefore, the shielding against neutrons is placed first to the background source and the one against photons is placed second closer to the protected object.

The total probability for a neutron to interact with matter is given by the sum of the individual cross section, i.e.

$$\sigma_{tot} = \sigma_{elastic} + \sigma_{inelastic} + \sigma_{capture} \cdot \quad (22)$$

In analogy to photons, then, a collimated beam of neutrons passing through matter will be exponentially attenuated

$$I = I_0 e^{-n \cdot \sigma_{tot} \cdot t} \cdot \quad (23)$$

## 4. The energy-loss spectrometer

### 4.1 High resolution electron scattering facility

The layout of the high resolution energy-loss system is shown in Fig. 8. This system allows the operation of the spectrometer in the so-called energy-loss mode. It permits measurements where the resolution of electron scattering experiments does not depend on the energy spread of the electron beam.

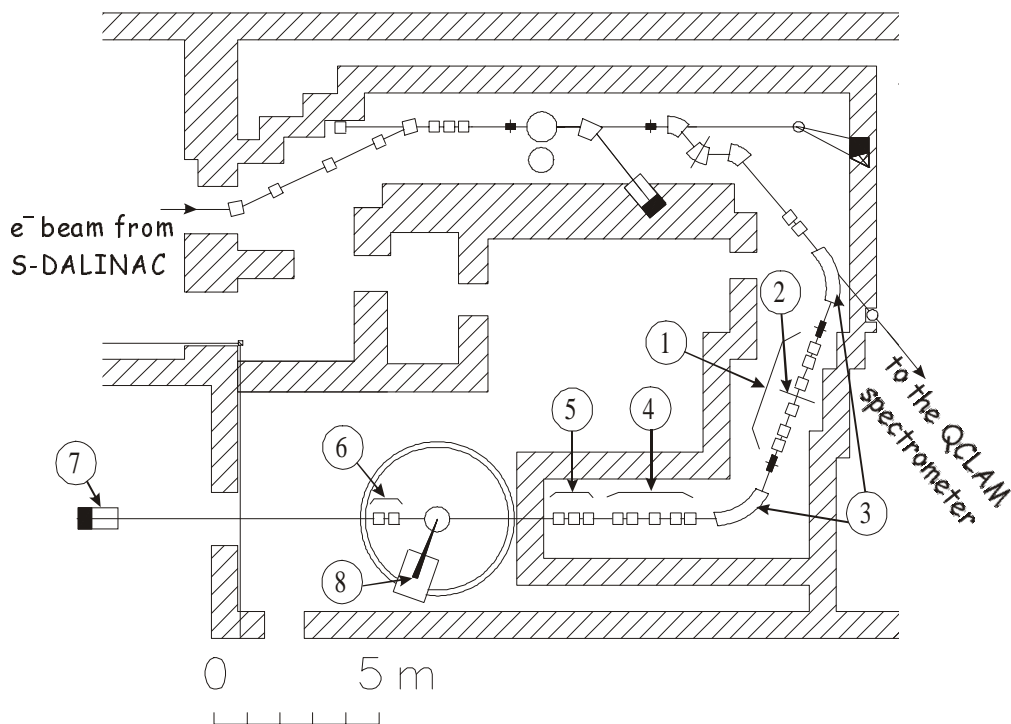


**Fig. 8:** High resolution energy-loss system.

- ① focussing quadrupoles, ② energy defining slit, ③ 70° bending magnets, ④ “rotator”, ⑤ focussing quadrupole triplet, ⑥ refocussing quadrupole doublet, ⑦ Faraday cup, ⑧ energy-loss spectrometer.

The system consists of six quadrupoles (Pos. 1) and two 70° bending magnets (Pos. 2) which form a momentum analyzing system with energy defining slits (Pos. 3) in the symmetry plane between these magnets. A set of five quadrupoles called “rotator” (Pos. 4), is used to turn at 90° the dispersion plane in the energy-loss mode of operation, and the quadrupole triplet (Pos. 5) focusses the

beam onto the target. A quadrupole doublet (Pos. 6) behind the target reduces the beam divergence due to multiple scattering and delivers it to a Faraday cup (Pos. 7) which simultaneously serves as current monitor. The scattered electrons are momentum analyzed in a high resolution magic-angle spectrometer (Pos. 8).

The energy-loss spectrometer is shown in Fig. 9. The electron beam from the accelerator hits the target which is placed inside the scattering chamber at the pivot-point of the spectrometer (Pos. 1). The scattered electrons pass the spectrometer entrance slit defining the accepted solid angle  $\Omega$ , and are deflected by the dipole magnet (Pos. 2) to an angle of  $\pi\sqrt{8/3} = 169.7^\circ$  (this angle is called “magic” for reasons discussed in Sect. 4.3). Then electrons come out through the output vacuum chamber (Pos. 4), having been focussed in the focal plane where the new detector system will be located [4].

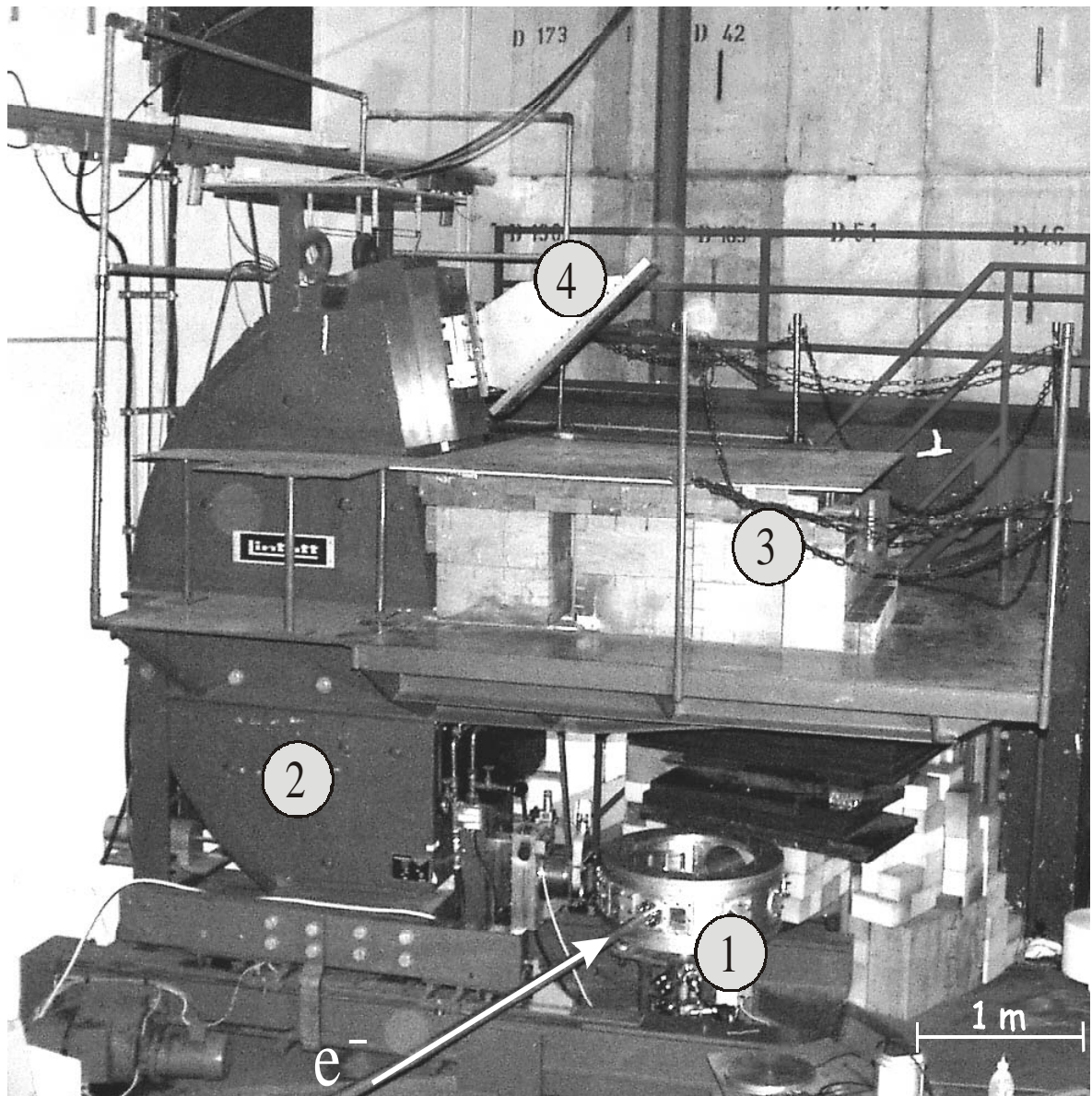


Fig. 9: The  $169.7^\circ$  spectrometer without detector system.

1 - scattering chamber, 2 - dipole magnet, 3 - paraffin and lead shielding, 4 - vacuum chamber.

The main parameters of the spectrometer are given in Tab. 2.

Tab. 2: Parameters of the energy-loss spectrometer.

---

---

Electron energy range	18 - 120 MeV
Angle range	25°-165°
Deflection angle	169.7° ± 0.1°
Radius of central trajectory	1.00 m
Solid angle acceptance	5 msr
Dispersion	4 cm /%
Field strength	0.6 - 4.0 kG
Weight	
spectrometer	17 t
shielding (safe load)	10 t

---

---

## 4.2 Matrix formalism and ion-optical properties of the spectrometer

In order to describe the behavior of charged particles passing through one or more ion-optical devices the concept of transfer coefficients is used [23]. The box in Fig. 10 represents any ion-optical transfer system consisting of magnetic dipoles, quadrupoles etc. A particle is assumed to be emitted from (or passing through) points  $X_1, Y_1$  in the plane  $Z_1 = 0$ . After having transversed the system, it will be detected at position  $X_2, Y_2$  in the plane  $Z_2 = 0$ . The direction of the particle before entering the system is specified by the angles  $\theta_1$  and  $\Phi_1$  defined in the figure. A reference momentum  $p_0$  is assumed, and the deviation from this momentum is given as  $\delta = \Delta p / p_0$ . For simplicity, it is assumed that the system is mechanically symmetric about the  $XZ$  - plane and that for  $Y = 0$  the magnetic field is perpendicular to this symmetry plane. At the energy-loss spectrometer it should be the symmetry plane of the dipole magnet.

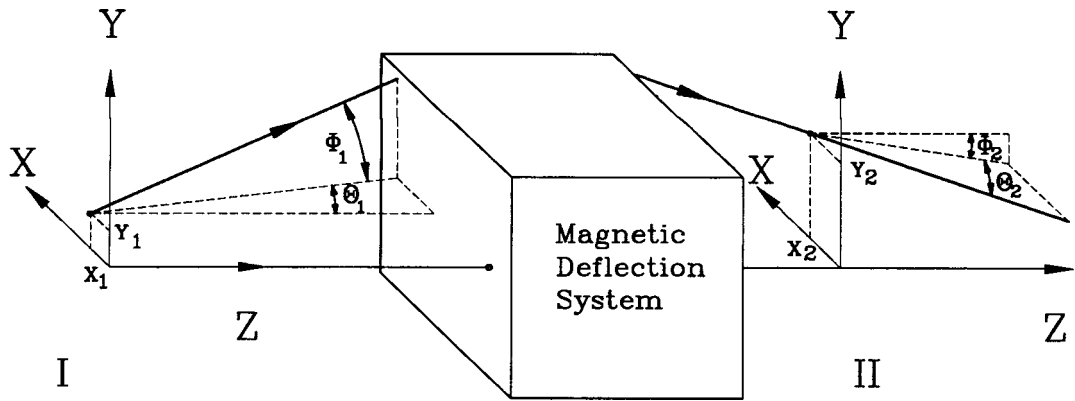


Fig. 10: Illustration of the coordinates for a calculation of a magnetic deflection system.

The electron beam position at the exit is a function of the position and direction at the entrance and of the momentum. Thus

$$X_2 = f(X_1, \theta_1, Y_1, \Phi_1, \delta) \quad (24)$$

with similar expressions for  $\theta_2$ ,  $Y_2$ , and  $\Phi_2$ . The exit coordinate system is chosen such that a particle with momentum  $p_0$  entering along the  $Z_1$  axis exits along  $Z_2$ . Then Eq. (24) can be expressed as a Taylor expansion in  $X_1$ ,  $\theta_1$ ,  $Y_1$ ,  $\Phi_1$ , and  $\delta$ :

$$\begin{aligned}
X_2 = & (X/X)X_1 + (X/\theta)\theta_1 + (X/\delta)\delta + (X/X^2)X_1^2 + (X/X\theta)X_1\theta_1 + \\
& + (X/\theta^2)\theta_1^2 + (X/X\delta)X_1\delta + (X/\theta\delta)\theta_1\delta + (X/\delta^2)\delta^2 + \\
& + (X/Y^2)Y_1^2 + (X/Y\Phi)Y_1\Phi_1 + (X/\Phi^2)\Phi_1^2 + \text{higher order terms.}
\end{aligned} \tag{25}$$

The factor  $(X/X)$ , called a transfer coefficient, is actually the first-order derivative  $\partial X_2/\partial X_1$ . Similarly, the term  $(X/\theta)$  is equal to  $\partial X_2/\partial \theta_1$ , etc. The term  $(X/X)$  is the magnification of the system in the  $X$  direction and  $(X/\delta)$  is the dispersion. This measures the displacement in the  $X$  direction at the exit per unit change in  $\delta$ .

### 4.3 Energy-loss mode

In the energy-loss mode the spectrometer is used in conjunction with the beam transport system (see Fig. 11). Its basic principle is to match the dispersion of this system to that of the spectrometer such that the entire apparatus (starting at the accelerator exit) is non-dispersive in the spectrometer focal plane. This makes the system sensitive only to the energy loss in the target and independent of the momentum spread of the beam.

The electron beam is projected on the target by the beam transport system described in Sect. 4.1 at different spots. The distance between them is defined by the beam energy spread  $\delta E$ . If the dispersion of the beam transport system and that of the spectrometer are matched then the electron beam is focussed onto the focal plane in one spot. If the electrons lose their energy by passing the target the spot in the focal plane is displaced by the distance  $\Delta x$  determined by the energy-loss value  $\Delta E$  of electrons in the target.

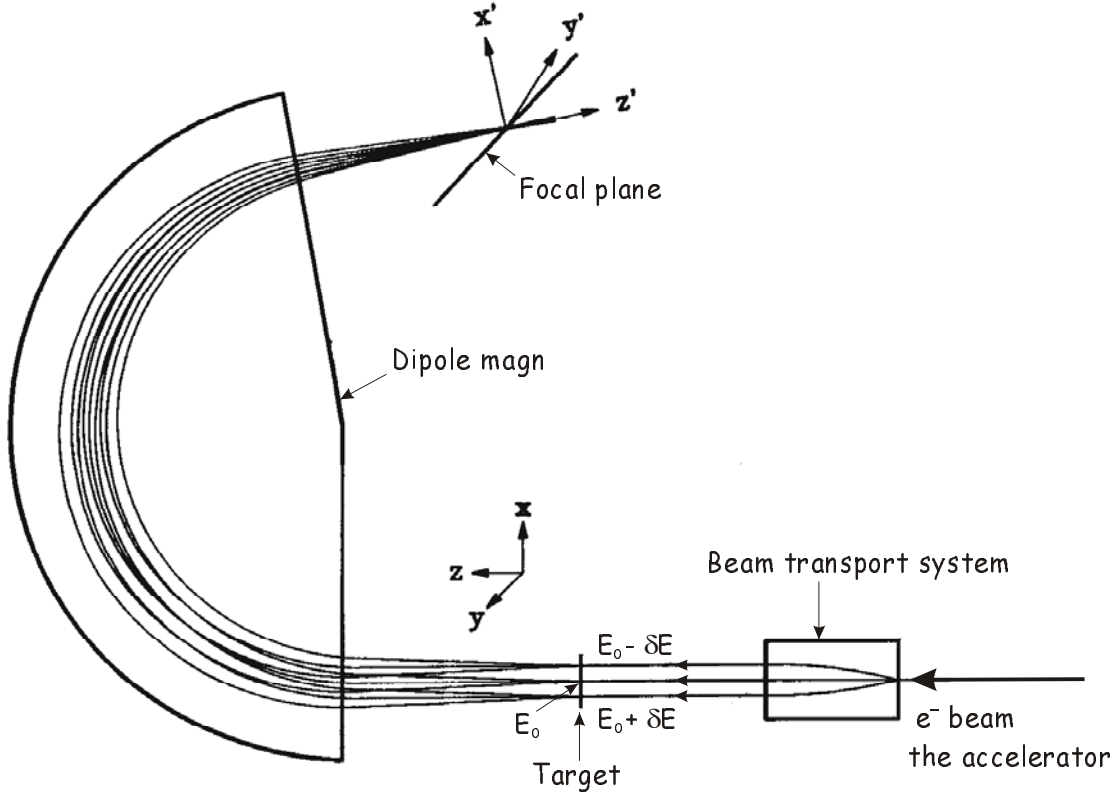


Fig. 11: Operation principle of the energy-loss mode.

The magnetic field in the spectrometer midplane can be described by the expansion

$$B_y = B_0 \left[ 1 - n(X/R_0) + \beta(X/R_0)^2 - \gamma(X/R_0)^3 + \dots \right] \quad (26)$$

with  $X = R - R_0$ , where  $X$  represents the radial distance and  $R_0$  the radius of the central trajectory, and  $n$ ,  $\beta$ ,  $\gamma$  are the first, second, and third derivatives of the magnetic field  $B$  with respect to  $R$ , respectively. Since  $n = 0.5$  is necessary to obtain double focussing, only  $\beta$  and  $\gamma$  are optional. To facilitate manufacturing conical pole shoe faces yielding  $\beta = 0.25$  and  $\gamma = 0.125$  were chosen. The deflection angle of  $169.7^\circ$ , together with the straight yoke edges at entrance and exit, is chosen such that the second order error ( $X/\theta^2$ ) vanishes for all object distances. The error ( $X/\theta\delta$ ) is eliminated by tilting the focal plane with respect to the central trajectory by an angle  $\alpha$  (see Fig. 12) given by

$$\tan \alpha = -\frac{(\theta/\theta)(X/\delta)}{(X/\theta\delta)}. \quad (27)$$

In the present system  $\alpha \approx 35^\circ$ .

Thus there is the possibility with a peak beam currents of up to  $20 \mu\text{A}$  and electron energies of up to  $120 \text{ MeV}$  to carry out electron scattering experiments with an energy resolution of about  $30 \text{ keV}$  [24].

#### 4.4 New detector system

Recently, a new focal plane detector system based on silicon microstrip detectors was developed for the energy-loss spectrometer [8]. The main advantages of these detectors are that they can be able to work with very high count rates, have very high resolution and an easy mechanical setup. The detector system for the scattered electrons consists of silicon microstrip detectors ( $4 \times 96$  strips) and a trigger detector (see Fig. 12).

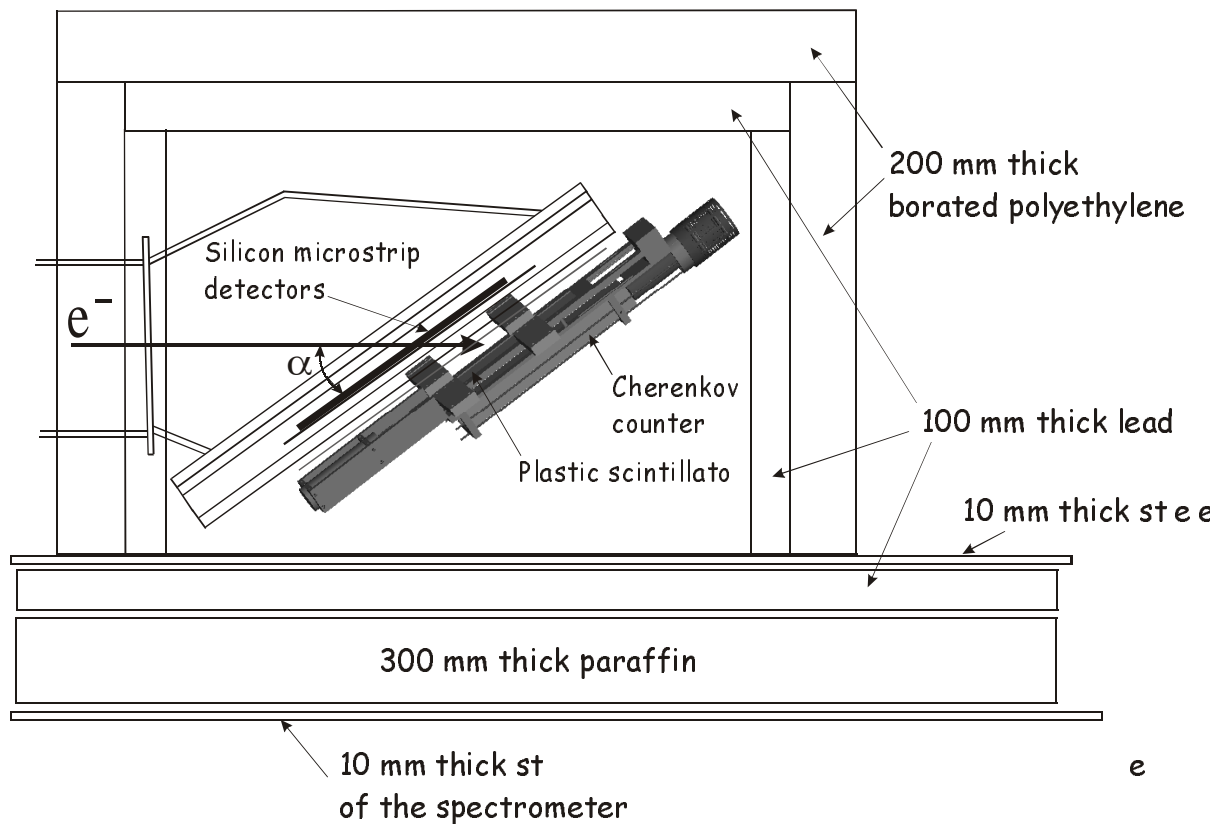


Fig. 12: New detector system with new shielding.

A plastic scintillator and a large Cherenkov counter serve as a trigger for background suppression. The spatial resolution of the semiconductor micro-strips is 0.5 mm which corresponds to  $\Delta E/E = 3 \times 10^{-5}$ . For comparison, at the QCLAM spectrometer which is operated in the conventional mode, in spite of the fact that intrinsic resolution of the Multiwire Drift Chambers (MWDC) which serve as focal plane detectors at the spectrometer is estimated to be  $2 \times 10^{-4}$ , energy resolution under typical experimental conditions is about  $8 \times 10^{-4} - 1 \times 10^{-3}$  and is basically determined by the energy spread of the beam and energy loss of electrons in the target [25].

## **5. Shielding design**

In order to determine the necessary amount of shielding material some estimates of the background radiation around the detector system were made. This defines together with conditions which are necessary for proper operation of the detector system the layout described below.

### **5.1 Background sources and estimates of total background radiation at the detector system**

The main background sources close to the spectrometer are shown in Fig. 13. These are the  $70^\circ$  bending magnet (Pos. 1), the target (Pos. 2), the post-target system (Pos. 3) consisting of the beam pipe having 20 cm in diameter and two focussing quadrupole magnets, and further downstream the Faraday cup (Pos. 4).

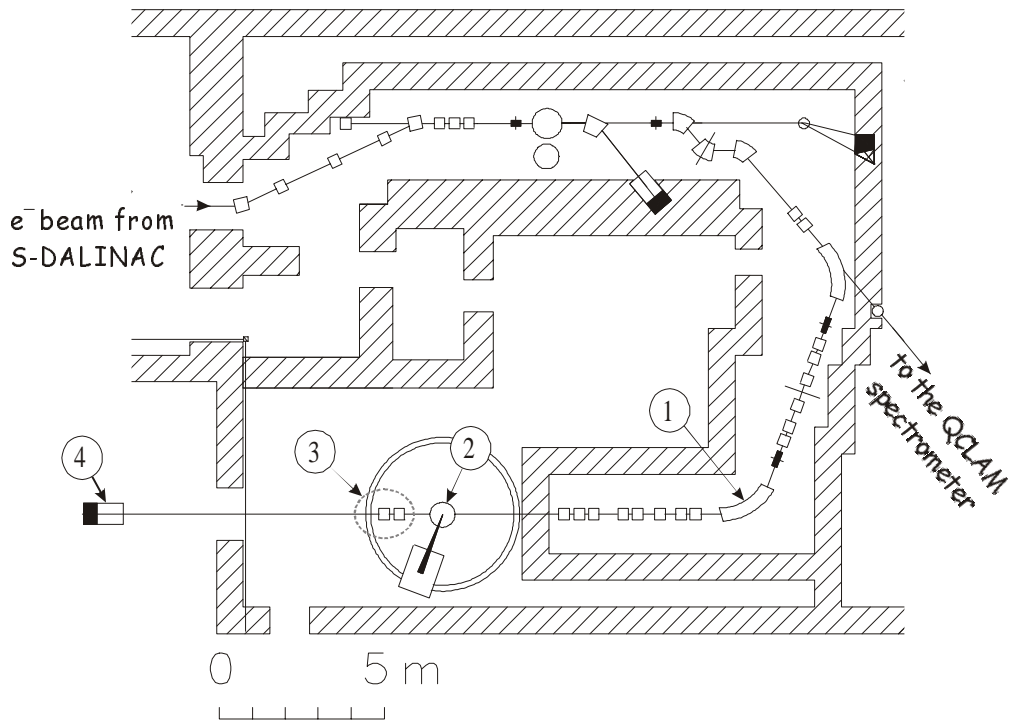


**Fig. 13:** Background sources close to the magic-angle spectrometer.

- ① 70° bending magnet, ② scattering chamber, ③ post-target system,
- ④ Faraday cup.

The Faraday cup is separated from the spectrometer by a concrete wall which is about 1 m in thickness followed by about a 30 cm thick paraffin brick wall. The post-target system is enclosed in an about 30 cm thick paraffin layer covered by about 20 cm thick borated polyethylene plates. With respect to the detector position between the 70° bending magnet and the spectrometer there is about 1 m of concrete. Previous experiments at the QCLAM spectrometer, where an identical beam stopper is used, have shown that the background from the Faraday cup can be neglected. Thus, it was necessary to estimate the total photon and neutron fluxes near the detector system created by the 70° bending magnet, the target and the post-target system.

To treat the problem of the estimates for the secondary particles yield analytically it is necessary to make the following simplifications:

1. The thin target approximation will be used instead of the thick target approximation for the calculation of the bremsstrahlung yield. This will result in an overestimate of yields because the yield scales with  $E_0$ .
2. The yield of bremsstrahlung photons at an angle of  $10^\circ$  is estimated using the relation  $\theta_0 \cdot E_0 = const$  with respect to the detector position solid angle that results in [26]

$$\frac{Y_\gamma(at\ 10^\circ)}{Y_\gamma(at\ 0^\circ)} \approx 10^{-1}$$

and at an angle of  $90^\circ$  by using the thick-target dose relation [26]

$$\frac{Y_\gamma(at\ 90^\circ)}{Y_\gamma(at\ 0^\circ)} \approx 10^{-3}.$$

3. Though the range of 130 MeV electrons is about  $26\text{ g/cm}^2$  [15], the effective range is assumed to be about  $5\text{ g/cm}^2$  because  $\gamma$  - radiation is reduced due to slowing down of electrons. Additionally the conversion efficiency to radiation is only about 50 %, as the radiation length  $L_{rad}$  in iron is about  $14\text{ g/cm}^2$  [22].
- These simplifying assumptions are chosen conservatively, i.e. rather over- than underestimating particle fluxes.

### 5.1.1 Photon and neutron yields from the 70° bending magnet

It is assumed that traversing the magnet, 10 % of the total electron beam are lost and hit the magnet wall passing a depth of 5 g/cm<sup>2</sup>.

**Tab. 3:** Input parameters for estimating the photon and neutron yields from the 70° bending magnet.

Electron energy	120 MeV
Electron current	2 μA
Target	steel
Target thickness	5 g/cm <sup>2</sup>
$\sigma_{\max}$	490 barns
$E_{\gamma 0}$	13.46 MeV
$\Gamma$	3.9 MeV
$E_{\gamma \text{ th}}$	7.37 MeV
$E_{\gamma \text{ max}}$	30 MeV

The number of photons per second produced in the bending magnet that reach the detector system can be written in the following way

$$Y_{\gamma} = Y_{\gamma}(\theta_0 = 10^{\circ}) \cdot \frac{\Delta\Omega}{4\pi} \cdot \exp\left\{-\frac{t_{\text{concrete}}}{TVL_{\text{concrete}}} \cdot \ln 10\right\}, \quad (28)$$

where  $Y_{\gamma}(\theta = 10^{\circ})$  is the total photon yield in the direction of the detector system. This is located at the angle of 10° with respect to the 70° bending magnet,  $\Delta\Omega$  is the solid angle of detector system,  $t_{\text{concrete}}$  is the thickness of concrete shielding. The value of  $Y_{\gamma}(\theta = 10^{\circ})$  was calculated using Eq. (10) and the data from Tab. 3.

The number of neutrons reaching the detector system can be estimated by the following expression

$$Y_n = Y_{n\ tot} \cdot \frac{\Delta\Omega}{4\pi} \cdot \exp\left\{-\frac{t_{concrete}}{TVL_{concrete}} \cdot \ln 10\right\}, \quad (29)$$

where  $Y_{n\ tot}$  is the total neutron yield. The total neutron yield  $Y_{n\ tot}$  was calculated using Eqs. (10, 16, 17) and the data given in Tab. 3.

### 5.1.2 Photon and neutron yields from the target

To estimate the contribution to background resulting from the target it is necessary to choose a case with maximum photon and neutron yields. Additionally it is necessary to take such real input parameters giving maximum possible yields of secondary particles from a target. A  $^{208}\text{Pb}$  target with a thickness of  $20\ \text{mg}/\text{cm}^2$  satisfies these requirements.

The detector system is located approximately at an angle of  $90^\circ$  relative to the beam axis and the target itself. The produced neutrons exhibit a roughly isotropic angular distribution and possess a Maxwellian energy distribution [see Eq. (18)].

Tab. 4: Input parameters for estimates of the photon and neutron yields for the target.

Electron energy	120 MeV
Electron current	20 $\mu\text{A}$
Target	$^{208}\text{Pb}$
Target thickness	20 $\text{mg}/\text{cm}^2$
$\sigma_{\max}$	490 barns
$E_{\gamma 0}$	13.46 MeV
$\Gamma$	3.9 MeV
$E_{\gamma\ \text{th}}$	7.37 MeV
$E_{\gamma\ \text{max}}$	30 MeV

The number of photons incident on the detector system will be approximately

$$Y_{\gamma} = Y_{\gamma}(\theta_0 = 90^{\circ}) \cdot \frac{\Delta\Omega}{4\pi} \cdot \exp\left\{-\left(\frac{t_{chamber}}{TVL_{steel}} + \frac{t_{platform}}{TVL_{steel}}\right) \cdot \ln 10\right\}, \quad (30)$$

where  $Y_{\gamma}(\theta_0 = 90^{\circ})$  is the total photon yield for the target at the angle of  $90^{\circ}$ ,  $t_{chamber}$  and  $t_{platform}$  are the thickness of the lid of the scattering chamber and the spectrometer platform, respectively. The value of  $Y_{\gamma}(\theta_0 = 90^{\circ})$  was calculated using Eq. (10) and the data given in Tab. 4.

The amount of neutrons reaching the detector system is given by the expression

$$Y_n = Y_{n\ tot} \cdot \frac{\Delta\Omega}{4\pi}, \quad (31)$$

where  $Y_{n\ tot}$  is the total neutron yield from the  $^{208}\text{Pb}$  target which is expressed using Eqs. (10, 16, 17) and the data from Tab. 4.

### 5.1.3 Photon and neutron yields from the post-target system.

Here it is assumed that after the electron beam passes the target, only 1 % of the electrons hits on the scattering chamber walls which again serve as an infinitely thick target as in the case discussed in Section 5.1.2.

Tab. 5: Input parameters for estimating the photon and neutron yields from the post-target system.

Electron energy	120 MeV
Electron current	0.2 $\mu$ A
Target	steel
Thickness	5 g/cm <sup>2</sup>
$\sigma_{\max}$	490 barns
$E_{\gamma 0}$	13.46 MeV
$\Gamma$	3.9 MeV
$E_{\gamma \text{ th}}$	7.37 MeV
$E_{\gamma \text{ max}}$	30 MeV

The number of photons that reach the detector system will be approximately

$$Y_{\gamma} = Y_{\gamma}(\theta_0 = 90^{\circ}) \cdot \frac{\Delta\Omega}{4\pi}, \quad (32)$$

where  $Y_{\gamma}(\theta_0 = 90^{\circ})$  is the total photon yield which is estimated using Eq. (10) with the input parameters given in Tab. 5.

The amount of neutrons reaching the detector system is given by the expression

$$Y_n = Y_{n \text{ tot}} \cdot \frac{\Delta\Omega}{4\pi} \cdot \exp\left\{-\frac{t_{\text{paraffin}}}{TVL_{\text{paraffin}}} \cdot \ln 10\right\}, \quad (33)$$

where  $Y_{n \text{ tot}}$  is the total neutron yield which is estimated using the Eqs. (10, 16, 17) and input parameters given in Tab. 5.

### 5.1.4 Total instrumental background

All the results of background yield estimates without a detector shielding are summarized in Tab. 6.

Tab. 6: Results of background yield estimates without a detector shielding.

<b>Background Source</b>	<b>Photon Yield [s<sup>-1</sup>]</b>	<b>Neutron Yield [s<sup>-1</sup>]</b>
70° bending magnet	$8.0 \times 10^4$	$2.8 \times 10^2$
Target	$2.5 \times 10^4$	$4.3 \times 10^2$
Post-target system	$2.3 \times 10^5$	$2.1 \times 10^4$
<i>TOTAL</i>	$3.4 \times 10^5$	$2.2 \times 10^4$

### 5.2 Requirements to the new shielding system

The new shielding system should satisfy the following requirements:

1. It should ensure attenuation of background radiation necessary for a proper detector operation within a high signal-to-noise ratio.
2. Assembling and disassembling should be easy to allow simple access to the detectors for maintenance and testing.
3. The total weight should be less than 10 tons because this is the safe load on the spectrometer platform.
4. The weight of individual pieces should not exceed 5 tons which is the maximum capacity of the crane available in the experimental hall.

### 5.3 Choice of the optimal shielding materials

In principle, any material can be used for radiation shielding if employed in a thickness sufficient to attenuate the radiation to the required level. The choice of the shield material depends on a number of factors, such as costs, final desired attenuated radiation levels, resistance to radiation damages, required thickness and weight, multiple use considerations, permanence of shielding, and availability.

It was already mentioned, that the attenuation of gamma rays and x-rays depends on the density of the shielding material; a dense shield material with a higher atomic number is a better attenuator of photons. Lead shields are frequently used where space is limited or where a compact area of absorbers is required. It is recognized that lead is not the densest element (e.g., tantalum, tungsten, and thorium are higher on the density scale), but lead is readily available, has a high degree of flexibility in an application, is easily fabricated and has by far the lowest cost of these materials.

The lead used as shielding material is usually an alloy with a few per cent of antimony which unfortunately is activated easily by  $(\gamma, n)$ , and  $(n, \gamma)$  reactions. However, the resulting background rates can be neglected with respect to the results of Tab. 6.

In choosing the material for the shielding against neutrons it is necessary to take into account the following fundamental neutron interactions processes:

1.  $(n, \gamma)$  capture dominant at thermal energies
2. resonant capture at keV-MeV energies
3. inelastic scattering important at MeV energies
4. elastic scattering important at MeV energies
5. nuclear reactions like  $(n, p)$ ,  $(n, \alpha)$
6. fission (not relevant here).

An ideal neutron shielding material is a combination of elements, which maximises the effects of these interaction processes over a wide range of neutron

energies. Thus, to make an efficient shield against neutrons it is necessary to use a mixture which contains

1. *hydrogen*, to slow down the fast- and intermediate-energy neutron by inelastic scattering,
2. *material with a sufficiently high thermal neutron capture cross section* in order to capture the neutrons efficiently after they slowed down. If possible, this material should not emit a very penetrating gamma ray after neutron capture; both, lithium and boron fulfil these requirements best,
3. *high density elements* to absorb the gamma rays formed in neutron capture and neutron inelastic scattering, and also to make the shield compact.

When taking into account the physical properties, easy fabrication and costs, polyethylene with 5-10 % of boron admixture is an optimal choice for neutron shielding in cases where a free space is limited.

In general, concrete is favoured for shielding around accelerators because cost effectiveness. However, this kind of shielding requires space and therefore is not applicable here.

The radiative fields of gammas and neutrons at an electron accelerator exhibit a complex energy distribution. The most important aspects can be summarized by considering the fast neutrons in the MeV range, thermal and epithermal neutrons, primary and secondary gammas. There are different types of shielding for each type of radiation.

Shielding for fast neutrons up to about 10 MeV is accomplished most efficiently by the use of elastic scattering on hydrogen nuclei. Hydrogen will also capture low energy neutrons, but this results in the undesirable emission of very penetrating secondary gamma rays. It is beneficial, therefore, to introduce an additional element which, even in low concentrations, is many orders of magnitude more effective than hydrogen in absorbing the thermal neutrons, but which emits no secondary radiations. Boron or lithium are elements with the most appropriate properties, and are most commonly used.

Thermal neutrons are neutrons in thermal equilibrium with their surroundings. Typical scattering of thermal neutrons does not generally change their kinetic energy. The upper limit of the thermal energy range is often taken as the cadmium cut-off energy of 500 keV. Thermal neutrons can be virtually eliminated by the presence of high thermal neutron cross-section materials such as boron, lithium, or cadmium.

Secondary gamma rays, with an energy of 2.2 MeV are arisen as a result of the capture of thermal neutrons by hydrogen. These capture gamma rays can be minimized by adding boron or lithium. Gamma rays resulting e.g. from capture of neutrons by boron have an energy of only 0.42 MeV which reduces the overall dosage considerably. Other materials should be avoided because they produce high energy  $\gamma$  - rays in the range of 3-5 MeV.

#### **5.4 Estimates of the necessary shielding thickness**

For a proper detector operation, the photon and neutron fluxes should be reduced as much as possible. In the development of the new shielding it is necessary to find a compromise between quality, cost and weight of the new shielding. The neutron yields presented in Tab. 7 are generally much lower than the photon yields. Thus, for an estimate it is necessary first to define the admissible photon flux through the detector system. It is defined by the maximum detector electronic read-out rate, the semiconductor detector charge saturation and the necessary signal-to-noise ratio.

As a starting point the experience gained at the QCLAM spectrometer can be used [27]. There a shielding of 10 cm thick lead and 20 cm thick borated polyethylene is employed which reduces the photon and neutron yields by a factor of about 110 and 20, respectively (see Tab. 1).

Tab. 7: Results of background estimates with a detector shielding.

---

---

<b>Background Source</b>	<b>Photon Yield [s<sup>-1</sup>]</b>	<b>Neutron Yield [s<sup>-1</sup>]</b>
70° bending magnet	$7.2 \times 10^2$	14
Target	$2.3 \times 10^2$	22
Post-target system	$2.1 \times 10^3$	$5.5 \times 10^2$
<i>TOTAL</i>	$3.1 \times 10^3$	$6.0 \times 10^2$

---

---

Since the energy distribution of the background gamma flux is unknown it is almost impossible to predict the semiconductor detector charge saturation. The read-out rate of the recently developed detector system is limited by 100 kHz. At the same time, the useful events rate under the typical experimental conditions does not usually exceed the 10 kHz level. Therefore, in the extreme case of 100 % microstrip detector efficiency for the background radiation a signal-to-noise ratio is estimated to be about  $1 \times 10^4 / 3.1 \times 10^3 \approx 3$ , which is just enough to extract relevant physical information from the data. In reality this ratio is expected to be much higher because of the trigger detector used for preventing the silicon detector from registration of other events than those from electrons by means of active background suppression.

## 6. Construction of the shielding

In the framework of this diploma thesis the new shielding has been designed. The shielding was constructed two-layered. The protection against photons is achieved by a 10 cm inner layer of lead bricks. The shield against neutrons consists of an outer layer of 20 cm borated polyethylene plates.

Since the total weight exceeds the limit of 5 tons, the lead shielding consists of four separated sidewalls and a cover. The dimensions have been chosen to provide some free space between the lead shielding and the detector system in order to allow future modifications of the detector system. The lead walls are built from standard bricks ( $200\text{mm} \times 100\text{mm} \times 50\text{mm}$ ) held together by U-steel frames shown in Fig. 14.

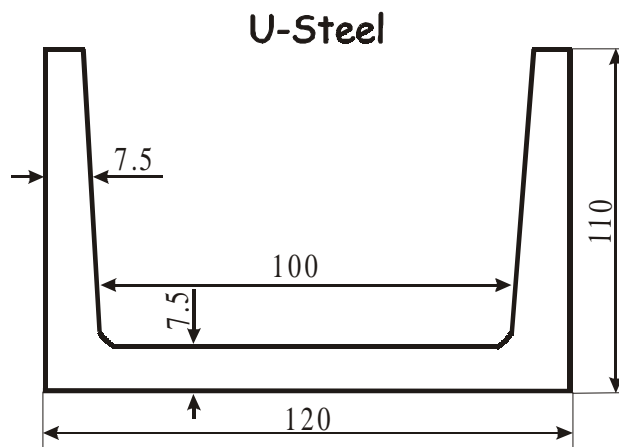
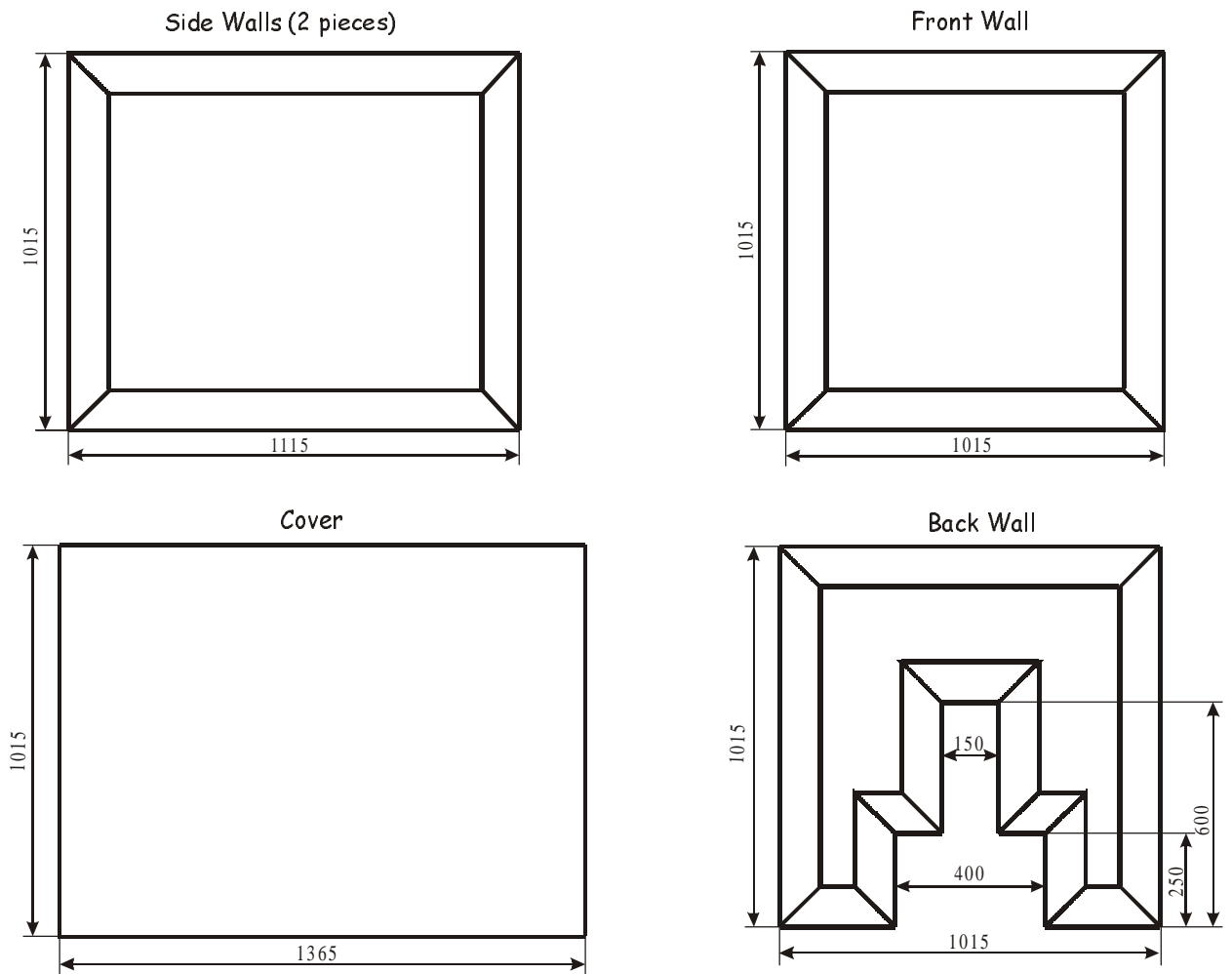


Fig. 14: Dimensions of a U-steel frame for supporting lead bricks in mm.

Drawings of the individual parts are shown in Fig. 15. The backside wall will be installed permanently to allow a fixed placement of the necessary detector cables. The other walls and the cover will be removable.



**Fig. 15:** Drawings of the individual U-steel frames for the lead shielding.

All dimensions in mm.

A three-dimensional view of the lead shielding is shown in Fig. 16. The steel strips which are also shown in the figure are necessary as an additional side support for the lead bricks. The sidewalls are connected with each other by means of iron angle.

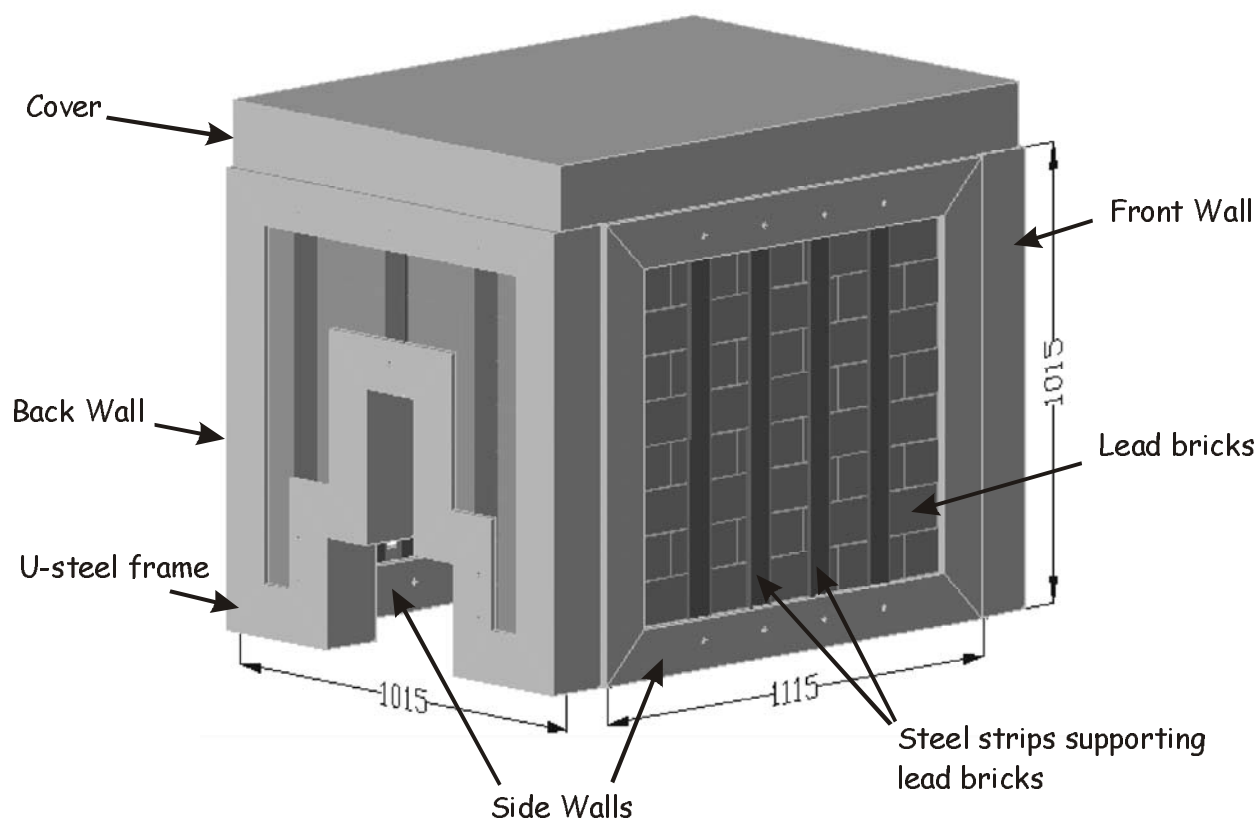


**Fig. 16:** Three-dimensional view of the new lead shielding.

The required amount of lead bricks for each piece and their total weight are given in Tab. 8. In total 540 lead bricks are needed. The lead shielding is surrounded with 20 cm borated polyethylene plates for the shielding against neutron. Their total weight is about 830 kg.

**Tab. 8:** Required amount of lead bricks for each piece and their total weight.

	<b>Required amount of bricks</b>	<b>Weight of the wall [kg]</b>
Side walls (2)	$110 \times 2 = 220$	$1247.4 \times 2$
Front wall	100	1134
Back wall	$\approx 85$	963.9
Cover	135	1530.9
<i>Total</i>	<i>540</i>	<i>6123.6</i>

## 7. Conclusion

In the framework of this diploma thesis a new passive shielding against neutrons and ionizing radiation produced by neighbouring background sources was designed for the detector system of the energy-loss spectrometer at the S-DALINAC. Estimates of the total background yields produced by the most important background sources like the 70° bending magnet, the target and the post-target system were presented. Based on these estimates and taking into account that the new shielding should attenuate the background down to a level at which the new detector system can operate properly the new shielding was designed. Furthermore, the construction enables a simple assembling and disassembling to provide an easy access to the detectors.

Estimates of the shielding thickness were carried out using experimentally measured shielding TVL parameters. The designed shielding consists of an inner 10 cm thick lead brick layer and an outer 20 cm thick borated polyethylene. The lead bricks walls are constructed using U-steel frames.

The shielding is currently under construction in the mechanical workshop and will be ready for use as soon as it is finished.

## 8. References

- [1] A. Richter, Prog. Part. Nucl. Phys. **44** (2000) 3.
- [2] P. von Neumann-Cosel, F. Neumeier, S. Nishizaki, V. Yu. Ponomarev, C. Rangacharyulu, B. Reitz, A. Richter, G. Schrieder, D.I. Sober, T. Waindzoeh, and J. Wambach, Phys. Rev. Lett. **82** (1999) 1105.
- [3] S. Strauch, P. von Neumann-Cosel, C. Rangacharyulu, A. Richter, G. Schrieder, K. Schweda and J. Wambach, Phys. Rev. Lett. **85** (2000) 2913.
- [4] H.-D. Gräf, H. Miska, E. Spamer, O. Titze, and T. Walcher, Nucl. Instr. Meth. **153** (1978) 9.
- [5] T. Walcher, R. Frey, H.-D. Gräf, E. Spamer and H. Theissen, Nucl. Instr. Meth. **153** (1978) 17.
- [6] D. Schüll, J. Foh, H.-D. Gräf, H. Miska, R. Schneider, E. Spamer, H. Theissen, O. Titze and T. Walcher, Nucl. Instr. Meth. **153** (1978) 29.
- [7] J. Foh, R. Frey, R. Schneider, A. Schwierczinski, H. Theissen and O. Titze, Nucl. Instr. Meth. **153** (1978) 43.
- [8] A. Lenhardt, Diplomarbeit, TU Darmstadt (1999).
- [9] A. Richter, Proceedings of the Fifth European Particle Accelerator Conference, ed. S. Meyers et al., (IOP Publishing, Bristol, 1996) 110.
- [10] J.C. Butcher and H. Messer, Nucl. Phys. **20** (1960) 15.
- [11] O.V. Bogdankevich, *Methods in Bremsstrahlung Research* (Academic Press, London, 1966).
- [12] W.R. Leo, *Techniques for Nuclear and Particle Physics Experiment* (Springer-Verlag Berlin Heidelberg, 1994).
- [13] Review of Particle Properties in Phys. Rev. **D45** , Part II (1992).
- [14] L.I. Schiff, Phys.Rev. **83** (1951) 252.
- [15] ICRU Report **37** (1984).
- [16] W. Miller, R.J. Kennedy, Radiat. Res. **4** (1956) 360.

- [17] D.A. Scag, *Discussion of radiographic characteristic of high-energy X-rays*, Nondestr. Test **12** (1954) 47.
- [18] K. Shure, J.A. O'Brien, D.M. Rothberg, Nucl. Sci. Eng. **35** (1969) 371.
- [19] S.S. Dietrich and B.L. Berman, Atomic Data and Nuclear Tables **38** (1988) 199.
- [20] M. E. Toms and W. E. Stephens, Phys. Rev. **108** (1957) 77.
- [21] S. Oki, Y. Takashima, M. Yamakage, H. Kibayakawa, K. Yoshida, K. Goto, Proceedings of the Second International Workshop on EGS, 8.-12. August 2000, Tsukuba, Japan, pp. 293-298.
- [22] W.P. Swanson, *Radiological Safety Aspects of the Operation of Electron Linear Accelerators*, IAEA Technical Report Series No. **188** (1979).
- [23] S. Kowalski, H.A. Enge, *RAYTRACE User's Guide*, Laboratory for Nuclear Science and Department of Physics, MIT, (1986).
- [24] T. Walcher, Habilitationsschrift, TH Darmstadt (1974).
- [25] Y. Kalmykov, private communication.
- [26] H. Dinter and K. Tesch, Deutsches Elektronen Synchrotron, Hamburg, Rep. DESY-76/19 (1976).
- [27] M. Knirsch, Dissertation, TH Darmstadt (1991), **D-17**.

## Acknowledgements

At this place I would like to thank several people who have contributed to the success of this work.

On the first place I would like to sincerely thank *Professor Dr. Dr. h.c. mult. Achim Richter* for given great opportunity to work on such an exciting topic under his supervision and to sense the climate of constructive team work in the modern scientific laboratory.

Further on I would like to thank *Privatdozent Dr. Peter von Neumann-Cosel* for numerous useful discussions during the realization of this diploma thesis and for the valuable remarks which he has made during the reading of this thesis.

I address my heartfelt gratitude to *Dr. Harald Genz* for his every day help, care and support.

I am grateful to *Dipl.-Phys. Alexander Lenhardt* for introducing me to the topic, his qualified and friendly patronage and for critical reading of this thesis.

I would like to express my gratitude also to *Dipl.-Phys. Yaroslav Kalmykov, Dipl.-Phys. Sergiy Khodyachykh, and Dipl.-Phys. Artem Shevchenko* for numerous significant advices.

I am grateful to *Dr. Shmatko, Dr. Shchus* and Chair of the Experimental Nuclear Physics of the Karazin Kharkiv National University (Ukraine) for the time they have spent for my education.

*Mrs. Sabine Genz* I would like to thank for the time she has spent on improving my English.

My special thank goes to the family Hartmann. Their warm and friendly attitude towards me helped me to feel at home here in Germany.

Finally, my heartfelt gratitude to my family – my parents *Mykola* and *Tetyana* and my sister *Julia*. Your thoughts and your care were supporting me very much during my study in the Karazin Kharkiv National University and during stay in Darmstadt.